HHS Public Access

Author manuscript

Biotechnol Bioeng. Author manuscript; available in PMC 2019 November 01.

Published in final edited form as:

Biotechnol Bioeng. 2018 November ; 115(11): 2793–2806. doi:10.1002/bit.26778.

Vascularized Microfluidic Platforms to Mimic the Tumor Microenvironment

Rhys Michna[1], **Manasa Gadde**[2], **Alican Ozkan**[1], **Matthew DeWitt**[3], and **Marissa Rylander**[1,2]

[1]Department of Mechanical Engineering, The University of Texas at Austin, 204 E Dean Keeton St, Austin, TX, 78712

[2]Department of Biomedical Engineering, The University of Texas at Austin, 107 W Dean Keeton St, Austin, TX, 78712

[3]School of Biomedical Engineering & Sciences, Virginia Tech, 325 Stanger St, Blacksburg, VA 24061

Abstract

Microfluidic technology has led to the development of advanced *in vitro* tumor platforms that overcome the challenges of *in vivo* animal and *in vitro* two dimensional models. This paper presents platform designs and methods used to develop complex vascularized *in vitro* models to mimic the tumor microenvironment. Features of these platforms include a continuous, aligned endothelium that allows for cell-cell interactions between vasculature and tumor cells. A novel platform for fabrication of a single endothelialized microchannel encased within a collagen platform hosting breast cancer cells was developed and utilized to study the influence of cellular interaction on transport phenomenon through vasculature in a hyperpermeable tumor microenvironment. This platform relies on subtractive tissue engineering fabrication techniques. Through confocal imaging we have demonstrated that the platform produces enhanced vessel leakiness recapitulating physiological features of the tumor microenvironment. The influence of tumor endothelial interactions on transport of particles was also demonstrated. Additionally, we designed two more complex and intricate endothelialized microfluidic networks by combining lithographic techniques with additive tissue engineering methods. We created a network platform consisting of interconnected microchannels to model a highly vascularized system and successfully perfused the system with fluorescent particles. Finally, we developed a physiologically representative *in vitro* microfluidic platform with vasculature patterned from *in vivo* data showing the versatility of these systems to replicate the complex geometries of tumor microvasculature and dynamically measured particle transport. Overall, we have shown the ability to develop functional microfluidic vascular tumor platforms of varying complexities and demonstrated their utility for studying spatial particle transport within these systems.

Graphical Abstract

Corresponding Author: Manasa Gadde, 204 E Dean Keeton St, ETC 7.134, Austin, TX, 78712, mgadde@utexas.edu, 408-406-8984.
Rhys Michna and Manasa Gadde are co first authors

Author Disclosure Statement: No conflict of interests exist.

Development of 3D vascular tumor microfluidic platforms from single vessel to complex in vivo patterned vascular platforms.

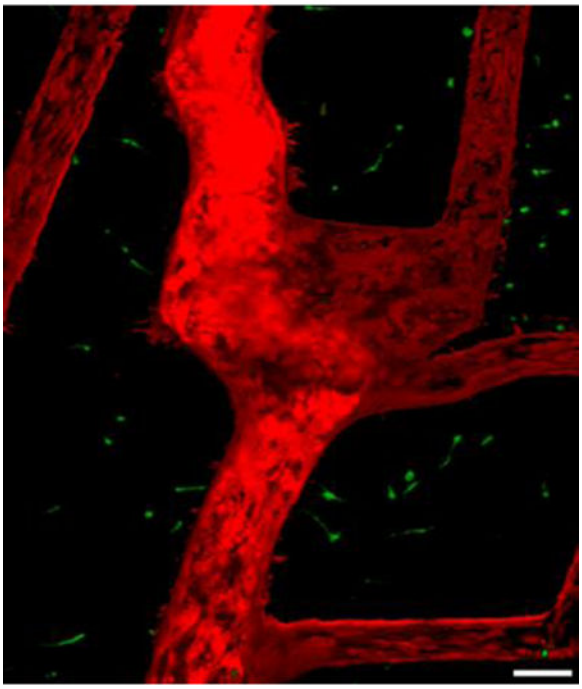

Introduction

The continuous development of new fabrication techniques in the field of tissue engineering is leading to creation of more advanced *in vitro* models to better understand the underlying influence of the microenvironment on human disease and tissue development. Three dimensional (3D) engineered tissue platforms have the ability to create physiologically representative features with an improved insight into the dynamic intricacies of the pathology of disease that is not possible with traditional two dimensional (2D) models (Buchanan et al., 2014b; Chrobak et al., 2006; Gadde et al., 2018; Golden et al., 2007; Griffith et al., 2006; Horning et al., 2008; Hutmacher et al., 2009; Ma et al., 2018; Mi et al., 2016; Soleimani et al., 2018; Staton et al., 2004; Sung et al., 2013; Sung et al., 2014; Yamada et al., 2007; Zhang et al., 2017; Zheng et al., 2012). Some of the features not simulated in 2D culture include but are not limited to cell-cell and cell-matrix signalling, transport studies, and impact of mechanical and chemical gradients on cellular response. Incorporation of microfluidic technology within 3D *in vitro* platforms allows long term cell culture and the ability to investigate the influence of flow and transport on dynamic cellular interactions in biological microenvironments (Buchanan et al., 2014b; Chrobak et al., 2006; Golden et al., 2007; Huang et al., 2017; Jeon et al., 2015; Zheng et al., 2012). These types of 3D models promote cell growth and migration and are playing a growing role in the study of cancer biology due to their ability to examine the influence of individual factors on tumor progression.

Hyperpermeability of the vasculature within the tumor environment along with a lack of lymphatic drainage is responsible for elevated interstitial fluid pressure that can dramatically alter flow patterns as the tumor expands (Azzi et al., 2013; Butler et al., 1975; Huang et al., 2017; Jain, 1988; Jain et al., 2014; Niederhuber et al., 2013; Vaupel et al., 1989). These hydrodynamic behaviours may lead to increased expression of angiogenic factors and formation of microvessels inside the tumor allowing for cancer growth while transport and drug uptake can be reduced by the fluid dynamics of the tumor vasculature (Azzi et al., 2013; Galmarini et al., 2000; Gkretsi et al., 2017; Jain et al., 2014; Jang et al., 2003; Multhoff et al., 2012; Tredan et al., 2007; Vaupel et al., 1989). Macromolecules and nanotherapeutics can fail to reach viable tumor cells due to the irregular extravasation and extravascular convection caused by the conditions of the tumor microenvironment. In order to study the influence of the vasculature on tumor development and transport of drugs, there has been a widespread expansion of *in vitro* platforms to incorporate channels to simulate vessels.

Collagen is commonly used as the extracellular matrix (ECM) component for creation of vascular channels in microfluidic devices (Charulatha et al., 2003; Drury et al., 2003; Parenteau-Bareil et al., 2010; Yamamura et al., 2007). Other proteins such as fibrin have also been used as scaffold material. Groups have utilized fibrin by itself or as a blend with different collagen percentages for various applications including cardiac, wound healing and cancer invasion studies (Chung et al., 2017; Lee et al., 2014; Mol et al., 2005; Nagaraju et al., 2018; Purtscher et al., 2015). However, low ultimate tensile strength of this material suggests it is not well suited for tissues of high stiffness such as breast tumor microenvironments, making collagen a more desirable scaffold material (Cummings et al., 2004). Other groups have used polylactic acid scaffolds in their *in vitro* studies to estimate chemotherapy toxicity in tumor microenvironment (Ma et al., 2012; Wang et al., 2006). However, using a non-protein based scaffold material limits physiological cell-matrix interactions, which affects proliferation and representative cell response (Antoine et al., 2014; Antoine et al., 2015). Groups have utilized subtractive and additive tissue engineering processes to form microfluidic collagen scaffolds (Bettinger et al., 2012; Bhatia et al., 2014; Peela et al., 2017; Tien, 2014). Scaffolds with complex microfluidic networks have also been formed using additive methods of combining layers of natural materials formed with lithographic techniques and have been used to investigate various behaviours such as cell-cell interactions during angiogenesis or metastasis, extravasation of breast cancer cells and interactions with the endothelium (Bhatia et al., 2014; Bischel et al., 2013; Farahat et al., 2012; Ghousifam et al., 2017; Jeon et al., 2015; Lee et al., 2014; Ma et al., 2018; Mi et al., 2016; Nagaraju et al., 2018; Peela et al., 2017; Price et al., 2008; Soleimani et al., 2018; Song et al., 2009; Zheng et al., 2012). While these microfluidic devices have provided insight into tumor behaviour, the *in vitro* platforms consist of small number of cells limiting the use of biological assays such as PCR or ELISA, or they lack a continuous endothelium failing to recapitulate the *in vivo* tumor microenvironment. In recent years, different methods have been proposed and discussed for the fabrication of microfluidic based vasculatures constructed within ECM. One method used frequently is to fabricate a housing to encapsulate, polymerize, and pattern collagen to create vasculature using sterile needles (Nguyen et al., 2013; Price et al., 2010; Tourovskaia et al., 2014; Wong et al., 2013; Wong et

al., 2010). Previously, the Rylander group has developed a platform to mimic vascular tumor microenvironments that overcomes planar geometries inherent to conventional PDMS based devices to produce a more physiologically representative 3D cylindrical endothelialized vascular microchannel (Buchanan et al., 2014a; Buchanan et al., 2014b; Szot et al., 2011, 2013). Fabrication of the platform relies on simple low cost methods to form an optimal *in vitro* environment for the formation of an endothelium and increased cellular capacity compared to other platforms dependent on lithographic methods. Although fluorinated ethylene propylene (FEP) tubing provided a robust infrastructure for maintaining vessel stability, the dimensions of the platform's tissue chamber were not scalable due to limitations set by using off the shelf FEP tubing. Additionally, introducing flow in the microchannel during live cell imaging presented challenges. The platform needed to be filled with water to match refractive indices in order to form an optically clear system for obtaining images. This requirement created the potential for leaks and limited resolution due to slight variations in refractive indices between multiple mediums in the platform.

Here we present a novel *in vitro* platform that capitalizes on the strengths and functionality of the Rylander group's earlier published platform for the creation of a single vessel vascularized tumor model. The new platform utilizes simplified fabrication techniques leading to increased reproducibility (Figure 1) while maintaining endothelial integrity using flow preconditioning method developed previously (Buchanan et al., 2014b). In contrast to current methods in literature, the housing material mold for this platform is fabricated using micro-milling techniques, decreasing both materials and time for fabrication and eliminating the requirement of multistep fabrication processes, and expensive reagents. Additionally, the platform does not rely on incorporation of micropillars similar to many groups for providing structural support to the collagen matrix endothelium or for separating cellular compartments, limiting the introduction of factors that deviate from the *in vivo* tumor-vasculature interface (Pagano et al., 2014; Prabhakarpandian et al., 2015; Sleeboom et al., 2018; Tsai et al., 2017; Vickerman et al., 2008). The new fabrication method enables creation of platforms that can be easily customized to alter geometries of the tissue chamber and vessel size while maintaining a continuous endothelialized lumen. The platform also establishes a simpler setup with new capability for high resolution, live cell imaging of particle transport in the tumor while allowing cell-cell interactions between tumor and vasculature. We demonstrate that a functional endothelium is formed in the tumor microenvironment and then investigate the influence of tumor interactions with the endothelium on particle transport across the endothelium.

This work also introduces the formation of more complex tumor microvascular network encased in a collagen hydrogel consisting of a co-culture of tumor and endothelial cells. The platform fabrication methods utilized in this study are based on works published by Zheng et al and tissue engineering techniques previously developed by the Rylander group (Buchanan et al., 2014a; Buchanan et al., 2014b; Szot et al., 2011; Zheng et al., 2012). While Zheng et al. focused on the interactions between endothelial and perivascular cells, we adapted the technique to recreate the tumor-vasculature interface with the incorporation of breast cancer cells in a collagen matrix with modulus representative of breast tumor tissue. Also, our work builds upon these studies by investigating particle transport through tortuous geometries with multiple vessel diameters representing different types of vessels. Lastly, we have

pioneered a novel platform with tumor vasculature re-created from *in vivo* data and to our knowledge, this is the first time this has been done. The works presented in this study lay the foundation for producing platforms that can create a tumor microenvironment for evaluation and development of new therapeutics and personalized cancer treatment plans.

Material and Methods

Platform Design and Fabrication:

Platforms of varying complexity ranging from single vessel platforms to vascular network platforms were fabricated using polycarbonate and PDMS housing components interfaced with glass cover slips to produce a tissue chamber with an imaging surface as shown in Figures 1a and Figure 2a. All polycarbonate and aluminium components used in fabricating the hydrogel scaffolds were computer numerical control (CNC) machined. The aluminium mold used for the single vessel platform holds a 22G needle and was used to form a PDMS chamber (Figure 1a-b) with an inlet and outlet for flow. For the network platforms, stainless steel 4–40 machine screws fixed the CNC machined polycarbonate network platform components together (Figure 2d). Standard soft lithographic techniques were used to produce patterned PDMS stamps for use in forming network platforms (Whitesides et al., 2001). For both single and network platforms, PDMS chamber and glass cover slip were bonded together by exposure to plasma treatment before being assembled.

Formation of Collagen Hydrogels:

A working collagen solution 7 mg/mL for use in the platforms was prepared by neutralizing stock collagen with a buffer composed of 10x DMEM, 1N NaOH, and 1x DMEM. This solution was added to the single vessel and vascular network platform chambers and polymerized for 25 minutes at 37^{O}C. For the single vessel platform, a 22G needle was left encased in the collagen during the polymerization process (Figure 1c). After removing the needle a hollow cylindrical microchannel remained (Figure 1d).

Fabrication of the vascular network platforms, as shown in Figure 2, was adapted from previously published protocols (Morgan et al., 2013; Wong et al., 2014; Zheng et al., 2012). The well in the base component of the platform was filled with collagen and then, a flat PDMS piece was laid on top of the well to produce a flat collagen surface after polymerization (Figure 2c). The well in the top component was aligned with a lithographically produced PDMS stamp (supplemental section S1) that had the designed channel pattern, and pins were inserted into the chamber to create an inlet and exit port before the chamber was filled with collagen and polymerized (Figure 2c). After polymerization and removal of the PDMS and pins, the top and bottom components of the platform were stacked resulting in a network fully encased in collagen (Figure 2d) into which endothelial cells were introduced. Once a confluent endothelium was established a circular cross-section is formed. The average diameter of tumor microvessels has been reported to be less than 100 μm (Niederhuber et al., 2013). However, seeding channels with a diameter of approximately 50 μm with endothelial cells causes cells to aggregate and clog the channels (Tien, 2014). Based on this information our stamps were designed to have diameters of 100 μm or greater.

Cell Culture:

To create the tumor microenvironment, MDA-MB-231 breast cancer cells labeled with green fluorescent protein (GFP) were suspended in the working collagen solution to the targeted density of 1×10^6 cells/mL and polymerized as described above (Buchanan et al., 2014a; Buchanan et al., 2014b; Szot et al., 2011, 2013). After polymerization of the collagen and the formation of vascular microchannels in the scaffold, red fluorescent protein (RFP) labelled telomerase immortalized microvascular endothelial (TIME) cells were injected into the microchannels. For the single vessel platforms, TIME cells (2×10^7 cells/mL) were injected twice at 10 minute intervals and the platform was slowly rotated to promote cell adhesion around the entire channel. To form a confluent endothelium the platforms were connected to a syringe pump providing a continuous flow of TIME cell media into the channels resulting in a wall shear stress (WSS, (τ)) of 0.01 dyn/cm^2 for 36 hours followed by 36 hours of 0.1 dyn/cm^2 (Figure 1e-f and 2e-f) following a previously established protocol (Buchanan et al., 2014b).

For the network plxatforms, 15 μL of media containing TIME cells (5×10^6 cells/mL) was added to the inlet and allowed to perfuse into the channels for 20 minutes at 37^{o}C. Flow for the vascular network platform was based on a reservoir system that depends on gravity creating a pressure difference at the inlet and outlet to induce a flow through the system (Figure 2g). The gravity reservoir preconditioning method required establishing a height difference of approximately 6 mm between the inlet and outlet reservoirs providing a decaying flow rate with the height difference reestablished every 12 hours.

Viability Analysis:

Viability of MDA-MB-231 breast cancer cells in the tumor platforms was evaluated using calcein AM (live)/propidium iodide (PI) (dead) (ThermoFisher Scientific) corresponding to green and red stains, respectively (Figure 4a). After completion of preconditioning the platform, unlabelled MDA-MB-231 cells in the collagen were incubated with 1μM calcein AM solution for 30 minutes followed by a 10 minute incubation in 45 μM PI solution. Samples were imaged immediately after PI treatment using Leica TCS SP8 confocal microscope.

Endothelium Morphology:

F-actin staining and SEM analysis was completed immediately following endothelial preconditioning to visualize endothelial morphology and orientation in the microchannels. For F-actin staining, the microchannels were perfused with 4% paraformaldehyde and 0.5% triton-X-100 (Sigma Aldrich) for 20 minutes followed by incubation in 1% bovine serum albumin for 30 minutes. Rhodamine Phalloidin (ThermoFisher Scientific) probe was used to label F-actin and imaged using Leica TCS SP8 confocal laser scanning microscope with HC PL Fluotar 10x/0.30 objective. SEM analysis was performed using a Zeiss Supra40 SEM-Electron Microscope. Microchannels were fixed overnight in an aldehyde mixture osmium treatment for 4 hours. Post fixation, the platforms were dehydrated in a series of ethanol solutions (50–70-95%), then critical point dried by CO_2 and coated with a thin layer of platinum-paladium.

Permeability:

Permeability coefficients were obtained to quantify the rate of transport through the endothelium of the microchannel in response to perfusion of 70kda dextran particles. Particles with a molecular weight of 70 kda are commonly used in transport studies and are comparable to large macromolecules (Chahine et al., 2009; Hoffmann et al., 2011). Three conditions of the single vessel platform were evaluated including an acellular microchannel, an endothelialized TIME microchannel without MDA-MB-231 cells, and a platform containing co-culture of TIME and MDA-MB-231 cells. Studies were conducted upon completion of the 72 hour preconditioning protocol. Green fluorescent dextran suspended in serum free endothelial basal media (EBM-2) at 10 μg/mL was perfused through the microchannels for 2 hours at a flow rate of 260 μL/min generating a WSS of 1 dyn/cm^2 with images being taken every five minutes for evaluation of transport and diffusion. In normal microvessels the average WSS is around 4 dyn/cm^2 (Buchanan et al., 2014a; Topper et al., 1999). The abnormal vasculature in tumors can compromise flow resulting in reduced WSS relative to normal blood capillaries and this led to the selection of a lower value of 1 dyn/cm^2 for particle transport studies (Kamoun et al., 2010).

Imaging for diffusion studies was completed on a widefield inverted Leica DMI 6000 B fluorescence microscope and the tiff images obtained were exported to MATLAB for evaluation. The average fluorescent intensity of the diameter of the collagen was measured and used to determine the diffusion permeability coefficient P_d. This coefficient describes the ability of solute to pass uniformly from the microchannel into the surrounding hydrogel and is calculated with the following equation:

$$P_d = \frac{1}{I_1 - I_b}\left(\frac{I_2 - I_1}{\Delta t}\right)\frac{d}{4} \quad (1)$$

where I_b is the background intensity, I_1 is the average initial intensity, I_2 is the average intensity after recovery time interval Δt, and d is the diameter of the microchannel (Price et al., 2011). The last five consecutive data points from the 2 hours of flow were used to calculate P_d as these were the time points at which stable and consistent measurements were achieved. Three samples (n=3) were collected for each variation in the diffusion studies. Data is expressed as a mean value ± standard deviation. Significance of the data was verified using Student's *t*-test and a 95% confidence criteria between groups of data. Blue 0.10 μm fluorescent polymer m particles were used to visualize particle transport in the network tumor platform to contrast against colors of labeled cancer and endothelial cells. The particles were suspended in serum free endothelial media at a density of 10 μg/mL and allowed to perfuse into the system for 1 hour.

Modeling Flow Inside the Vasculature:

WSS is one of the key factors in creating physiological *in vitro* tumor microenvironments (Buchanan et al., 2014a; Buchanan et al., 2014b). In order to estimate WSS, velocity profile inside vasculature needs to be determined. Velocity profiles were calculated using by

modelling flow inside vasculature networks using Comsol Multiphysics. Stokes law was used to quantify the flow inside the vasculature with the following assumptions: constant fluid viscosity, incompressible fluid, and a low Reynold's number inside the vasculature (Landau et al., 1987).

$$\rho\frac{\partial u}{\partial t} = \nabla P + \mu\nabla^2 u \quad (2)$$

where ∇ is gradient operator and ∇^2 is the square of vector Laplacian, P is pressure, u is velocity, μ is viscosity and ρ is density of the fluid. Simulations were run on the network platforms with the following conditions: constant flow rate of 15 μl/min at inlet and outlet boundary condition of zero gauge pressure. Other ECM properties used in the simulation were porosity of collagen of 0.49 and permeability of collagen of 10×10^{-15} m^2 (Serpooshan et al., 2013). Resulting flow velocity profile was used to calculate WSS at the vessel walls. WSS of a Newtonian fluid is defined as:

$$\tau = \mu\frac{\partial u}{\partial y}\Big|_{wall} \quad (3)$$

where u is velocity parallel to the vessel, and y is the perpendicular direction to the wall.

Results and Discussion

Single Vessel Platform Fabrication:

In this study, design changes have been made to the original platform developed by the Rylander group to create a more robust platform with greater capability to achieve high resolution spatial and temporal imaging of particle transport in a hyperpermeable tumor microenvironment resulting from tumor-vasculature interactions (Buchanan et al., 2014a; Buchanan et al., 2014b). In previously published work, an optically clear platform was obtained by filling a petri dish with water to surround FEP tubing structure that housed the tumor (Figure 3a). The geometry and size of the tissue chamber were previously restricted by the FEP tubing, and working with an open fluid on a microscope could introduce challenges. The new platform overcomes these complications while still creating a viable *in vitro* tumor microenvironment that can easily interface with imaging setups to complete studies of the microenvironment. The bonding of a PDMS chamber directly to a glass cover slip allows the hydrogel to be positioned closer to microscope objectives and eliminates the necessity of using water to create an optically clear system for imaging. Water removal from the platform decreased the necessary microscope working distance by over a millimeter (Figure 3a-b) and prevented potential fluid leaks while imaging. Inlet and outlet needles for flow are positioned more securely and promote a more stable platform for use on microscope stands. Using aluminium molds to form a PDMS tissue chamber and needles to form the microchannels enables scaling of the tissue chamber and channel dimensions

(Figure 3b). Therefore, platform size can be adjusted to create other interconnected vascularized tissues in addition to a single tumor platform (Figure 3c) not possible in the previous platform

Introducing different size platforms within the same device enabled creation of a simple body on a chip platform consisting of multiple chambers with unique vascularized tissue types. Endothelialized microchannels of different diameters have been fabricated using 22, 25, and 30 gauge needles corresponding to vessel diameters of approximately 717, 514, and 311 μm respectively (Figure 3d-f). This allows for a range of vessels sizes relevant to mammary tumor capillaries in the venous network to be mimicked (Less et al., 1991). The single vessel platform was also expanded upon to create a dual-channel platform (Figure 3g-h) capable of investigating the influence of pressure and biochemical gradient factors on tumor development and cell migration.

Engineered Tumor Microenvironment:

The *in vitro* tumor platforms are composed of MDA-MB-231 cells in a collagen ECM with a cylindrical and confluent endothelium as shown in Figure 4c, e, f. Following 72 hour flow preconditioning protocol, the TIME cells proliferated and elongated in the direction of flow as illustrated in Figure 4b. The nominal outer diameter of a 22 gauge needle is 717 μm. After removal of the needle, and sustained WSS during preconditioning, the final channel diameter could vary from the original of 717 μm to 900μm. Collagen channels seeded with endothelial cells have been reported to expand to larger diameters after 3 days of preconditioning (Chrobak et al., 2006). In order to confirm the capability of the platform to sustain the of cells, viability of the tumor cells was examined to determine if the bonding of a glass cover slip to the PDMS chamber created an oxygen deficient environment. The strong green fluorescence signal (live cells) with minimal red signal (dead cells) from both the endothelial cells and cancer cells in the collagen matrix revealed that the cells were viable and unaffected by being cultured in an enclosed PDMS chamber (Figure 4a). SEM analysis of the endothelial channels shows that they remain patent following the 72 hour flow preconditioning protocol without the need for structural support as shown in Figure 4e, f.

The morphology of the endothelial layer for mono and co-culture platforms was visualized using F-actin staining as evidenced by red fluorescence. Top view of the tissue chamber (Figure 4) shows tight endothelium for the TIME mono-culture (Figure 4b); however, leakier endothelium with gaps and holes in the endothelium (Figure 4d) was observed for the microchannel when endothelial cells were co-cultured with cancer cells as is also evidenced *in vivo* (Chauhan et al., 2012; Fukumura et al., 2007; Jain, 1988; Jiang et al., 2017; O'Brien et al., 2007; Vaupel et al., 1989). The large gaps and holes throughout the endothelial layer occur due to the interactions between the cancer and endothelial cells. Previous studies have revealed that direct contact between endothelial and cancer cells decreases endothelial viability (Kebers et al., 1998; Singleton, 2014; Zervantonakis et al., 2012a).

Transport:

To add quantitative support to the confocal images showing endothelial leakiness in the single vessel platform the vessel's permeability and to show the capability of these platforms for measuring dynamic and spatial transport, particle permeability was measured and permeability coefficient quantified. A progression of images flowing 70 kda dextran (260 μl/min) over a period of 2 hours shows an increase in the amount of dextran collecting in the collagen ECM for each condition compared to the zero time point. During optimization of the experimental setup, 2 hours was selected as a timeframe for allowance of a steady state permeability rate to be achieved. As expected, the acellular platforms without the presence of an endothelium exhibited the highest effective permeability coefficient average, 26±3 nm/sec with the most dextran transported into the collagen ECM, followed by the co-culture with an effective permeability coefficient of 25±1.7 nm/sec. Whereas the average value of the effective permeability coefficient for the mono-culture (endothelium only) was significantly lower ($p<0.05$) compared to the other 2 conditions with a permeability of 16±1.9 nm/sec which results from the barrier function of the endothelium. The intensity inside the channel itself does not change as the dextran is perfused under continuous flow. The higher intensity areas in the center of the 120 minutes (Figure 5) result from the collection of light from dextran that has diffused through the bottom and top of the channel. The vessel permeability data re-enforces our conclusions from the F-actin staining studies. The tight endothelium that forms in the mono-culture vascularized platforms serves to limit the amount of transport into the collagen ECM. The inclusion of cancer cells creates a leaky endothelium (Figure 4d) with pores allowing for increased transport out of the channel into the surrounding tissue resembling the well-known enhanced permeability effect (Buchanan et al., 2014a; Hashizume et al., 2000; Zervantonakis et al., 2012a). The extent of the leakiness formed in the co-culture platform prevents it from being significantly lower than acellular platform. The endothelium permeability properties influence the transport and effectiveness of particles and therapeutics into the targeted tumor site.

Others studies have reported similar results that the presence of tumor cells modulates the endothelial barrier function and increases transport of macromolecules through the endothelium into surrounding tissue (Buchanan et al., 2014a; Singleton, 2014; Zervantonakis et al., 2012a). It is expected that introducing particles larger than dextran (>70 kda) would decrease the diffusion rate through the endothelium and into the platform. Therefore, particles would congregate along the endothelial wall unable to pass through smaller gaps on the endothelium. Also, it is expected that increasing the particle size would increase the difference between co-culture diffusion and a non-endothelialized channel, as the co-culture endothelium is expected to be sufficiently confluent to prevent diffusion of larger sized particles.

Network Platforms:

To create an *in vitro* platform that better recapitulates a more vascularized tumor microenvironment and allows for tumor-ECM-endothelial interactions, we fabricated a microfluidic vascular network that enables improved perfusion and has the capability to scale the platform to larger tumor sizes. Using soft lithography, a simple geometric pattern was imprinted into collagen to form a network of channels encased in the platform. The

network has one inlet and outlet to provide transport through the system. The width of each channel was approximately 100 μm. Seeding TIME cells into the network followed by perfusion through the vessel resulted in a confluent endothelium throughout the network as shown in Figure 6. By suspending MDA-MB-231 cells in the collagen, a 3D *in vitro* engineered microfluidic vascularized tumor was created as presented in Figure 6a.

Evaluation of a top view of the co-culture network platform in Figure 6b shows endothelial behaviour similar to that of the single vessel platform in which the cells proliferate and elongate to form a confluent endothelium. The MDA-MB-231 cells interact with the endothelial cells to create gaps forming leakier endothelium as evidenced by the endothelium in Figure 6b. It was also observed that the use of collagen as a scaffold allows the TIME cells in the channels to remodel their surroundings resulting in final geometries that deviate from the strict rectangular geometry of the PDMS stamp pattern that other groups are limited too. The corners at microchannel intersections develop a circular radius allowing for a continuous endothelium as opposed to the squared PDMS corners as shown in Figure 6c, d, g. Fabrication of channels smaller than 100 μm diameter did not form a confluent endothelium as effectively through the entire network as the seeding of endothelial cells tended to clog the passageways. Similar findings have reported a minimum channel diameter of approximately 50 μm as the limit for this endothelialization process (Tien, 2014). The channels in our network remained patent (Figure 6h) and capable of transport after the preconditioning and this was verified by flowing blue 0.10 μm polymer particles through the network (Figure 6e). For the first time, we were able to track particle transport through the leaky *in vitro* tumor-vascular microenvironment in real time and observed even distribution throughout the network. It has been reported that shear stress plays a significant role in cell expansion, angiogenic response and metastasis (Buchanan et al., 2014a; Buchanan et al., 2014b; Galie et al., 2014; Shin et al., 2012; Verbridge et al., 2010). Simulation results (Figure 6f) demonstrate the capability to generate different velocity magnitudes in each vessel. Due to different velocity magnitudes in each vessel, WSS varies between 0.75–6.56 dyn/cm^2, which is within physiological WSS range reported in literature. As evidenced in Figure 6, the capability of the platform to dynamically track particle movement can be expanded to investigate the transport of chemotherapeutic or nanoparticle delivery in a hyperpermeable tumor microenvironment caused by the tumor-endothelial interactions.

In vitro platforms that re-create physiologically relevant tumor vasculature tailored to an individual allows for evaluation and optimization of patient specific therapies (Prabhakarpandian et al., 2015; Pradhan et al., 2018). In these platforms, transport of therapeutics could be studied in realistic environments and properties optimized to achieve targeted and efficient drug localization but limited work has been done to re-create tumor specific geometries. Following the initial vascular network pattern presented in Figure 6, a novel microfluidic network with tortuous geometry composed of collagen ECM was fabricated to replicate vasculature patterns found in representative *in vivo* tumors. An image of *in vivo* rat tumor vasculature was selected as a model to recreate and test the capabilities of this additive tissue engineering method for creating complex geometries (Figure 7a (Tong et al., 2004)). The *in vitro* platform presented in Figure 7b mimicked the geometry of the vasculature. The design consists of one large channel with a width and depth of

approximately 200 μm and multiple smaller branching channels with widths and depths of approximately 100 μm. Preconditioning of TIME cells in the channels remodelled the collagen to produce rounded corners and channel diameters of approximately 200 and 100 μm. Figure 7c shows FEA simulation results of velocity magnitude inside the *in vivo* vascular patterned platform with WSS varying between 0.75–2.55 dyn/cm^2. Similar to network platform, simulation results show physiological shear stress inside the *in vivo* vascular patterned platform. For the first time, transport of two different sized particles in an *in vivo* vascular patterned platform was investigated and presented in Figure 8 and 9. Figure 8 illustrates transport of 70 kda green fluorescent dextran, a common marker for protein and drug permeability, through the platform and diffusion into the surrounding ECM. Tumor region in between multiple vessels is saturated with dextran within the 30 minutes of perfusion but it takes over an hour to penetrate further into the collagen ECM. This transport behaviour is representative of drugs and chemotherapies having a harder time penetrating into the dense tumor ECM and reaching cells farther from the blood vessels *in vivo,* especially for abnormal, heterogeneously distributed tumor networks as demonstrated in this study (Grimes et al., 2016; Whatcott et al., 2015). In addition to dextran, the platform was also perfused with 0.10μm blue particles as shown in Figure 9. As the particle travel through the platform, they aggregate at the boundaries of the endothelium as seen in Figure 9b and c. We have shown earlier that co-culture of tumor and endothelial cells results in a leaky vasculature but as evidenced in Figures 8 and 9, while vessel leakiness can influence transport of small molecules like dextran, transport of larger particles is dependent on additional parameters such as hydrodynamic diameter as shown by previous in vitro permeability studies (Ho et al., 2017; Zervantonakis et al., 2012b). While this fabrication technique is capable of creating networks with complex geometries and multiple microchannel mimicking *in vivo* cases, it does present certain limitations. Lithography techniques can be used to create complex and detailed patterns; however, transferring these patterns to a collagen hydrogel is challenging. In order to capture the tortuous geometry in Figure 7, a lower, less viscous, collagen concentration of 6 mg/mL was used. Using lower collagen concentration increased the reproducibility of the hydrogel's ability to better encase the tortuous geometries of the PDMS pattern but was still unable to capture the smallest spatial geometries. Often, hydrogels fill large areas and focus on hosting small voids as opposed to the inverse case circled in Figure 7a that failed to be reproduced *in vitro* in Figure 7b. Another limitation of using lithographic techniques is that there is no means to create a gradual transition from larger to smaller channels, i.e. 100 μm channels connecting to 200 μm channel at a blunt interface. However, despite this interface, cells were capable of forming a confluent endothelium which is an important factor for transport studies. Also, increasing the number of microchannels with varying diameters quickly elevates the complexity of fabrication. Advances in 3D bioprinting are an alternative method for improved and fast fabrication of customizable advanced networks that move beyond the planar limitations of lithography (Bertassoni et al., 2014; Kolesky et al., 2014).

In this study, we present three different vascular platforms, single vessel, network and for the first time, an *in vivo* patterned platform consisting of a co-culture of tumor endothelial cells. Using these platforms, we mimicked the leaky vasculature present in the tumor microenvironment and studied the influence of the leaky vasculature on transport of particles

representative of chemotherapeutics and nanoparticles. We present methods for the fabrication of microfluidic channels by employing additive and subtractive tissue engineering techniques. The vascularized tumor platforms were created with embodiments of scalable channels (single/dual) and networks based upon *in vivo* vasculature. The single vessel platform, a modification on our previously published work, provided higher resolution imaging, a more robust infrastructure, and increased platform fabrication reproducibility. Utilizing this platform, we dynamically tracked tumor-vasculature interactions as well as the spatiotemporal behaviour of particle diffusion in a physiologically representative hyperpermeable tumor microenvironment. The network platform was designed to represent a highly vascularized tumor tissue. We built upon our observation in the single vessel platform and recreated the tumor-ECM-endothelial interactions as well as tracked transport of larger particles to mimic transport of nanoparticles through the tumor vasculature. Finally, for the first time, we recreated *in vivo* vasculature derived from rat tumor in an *in vitro* platform composed of tumor-endothelial co-culture in a collagen ECM representative of breast tumor tissue. The *in vivo* vascular platform consists of multiple branching vessels of varying diameters increasing the complexity of the vasculature present in the single and the network. Using the *in vivo* vascular platform, we tracked the transport of two different particles in real time. While we used data derived from a rat tumor, the platform can be designed to replicate patient data and allow for the study of transport and drug delivery in conditions that mimic the patient's tissue and delve further into the tumor-endothelial interactions revealed in the single channel platforms. These platforms form a foundation for the future study of drug transport, chemical gradients, and cell behaviour in a physiologically relevant tumor microenvironment. The single channel and network platforms, while providing a more simplistic tumor microenvironment, allow us to tease out the influence of individual factors such as cell-cell, cell-ECM, and growth factor gradients. The *in vivo* vascular pattern platform provides a more complex tumor microenvironment that can build upon the observations from the single and network platforms and observe them in a more physiologically relevant tumor environment. All these platforms can be expanded upon to incorporate immune cells, stromal cells, and lymphatic vessels to create a complete tumor microenvironment and be used to evaluate the toxicity of chemotherapeutics and lead to the development of new therapies.

Supplementary Material

Refer to Web version on PubMed Central for supplementary material.

Acknowledgements:

We would like to acknowledge our generous funding from NSRDEC and provided by Kris Senecal (US Army, RDECOM, Natick Research Development and Engineering Center, Natick MA), National Institute of Health Grant R21EB019646, Cancer Prevention Research Institute of Texas Grant RR160005.

References

Antoine EE, Vlachos PP, & Rylander MN (2014). Review of collagen I hydrogels for bioengineered tissue microenvironments: characterization of mechanics, structure, and transport. Tissue Engineering Part B: Reviews, 20(6), 683–696. [PubMed: 24923709]

Antoine EE, Vlachos PP, & Rylander MN (2015). Tunable Collagen I Hydrogels for Engineered Physiological Tissue Micro-Environments. PLoS One, 10(3), e0122500. [PubMed: 25822731]

Azzi S, Hebda JK, & Gavard J (2013). Vascular permeability and drug delivery in cancers. Front Oncol, 3, 211. doi:10.3389/fonc.2013.00211 [PubMed: 23967403]

Bertassoni LE, Cecconi M, Manoharan V, Nikkhah M, Hjortnaes J, Cristino AL, … Khademhosseini A (2014). Hydrogel bioprinted microchannel networks for vascularization of tissue engineering constructs. Lab Chip, 14(13), 2202–2211. doi:10.1039/c4lc00030g [PubMed: 24860845]

Bettinger C, Borenstein JT, & Tao SL (2012). Microfluidic Cell Culture Systems: Elsevier Science.

Bhatia SN, & Ingber DE (2014). Microfluidic organs-on-chips. Nat Biotechnol, 32(8), 760–772. doi: 10.1038/nbt.2989 [PubMed: 25093883]

Bischel LL, Young EW, Mader BR, & Beebe DJ (2013). Tubeless microfluidic angiogenesis assay with three-dimensional endothelial-lined microvessels. Biomaterials, 34(5), 1471–1477. doi: 10.1016/j.biomaterials.2012.11.005 [PubMed: 23191982]

Buchanan CF, Verbridge SS, Vlachos PP, & Rylander MN (2014a). Flow shear stress regulates endothelial barrier function and expression of angiogenic factors in a 3D microfluidic tumor vascular model. Cell Adh Migr, 8(5), 517–524. doi:10.4161/19336918.2014.970001 [PubMed: 25482628]

Buchanan CF, Voigt EE, Szot CS, Freeman JW, Vlachos PP, & Rylander MN (2014b). Three-dimensional microfluidic collagen hydrogels for investigating flow-mediated tumor-endothelial signaling and vascular organization. Tissue Eng Part C Methods, 20(1), 64–75. doi:10.1089/ten.TEC.2012.0731 [PubMed: 23730946]

Butler TP, Grantham FH, & Gullino PM (1975). Bulk transfer of fluid in the interstitial compartment of mammary tumors. Cancer Res, 35(11 Pt 1), 3084–3088. [PubMed: 1182701]

Chahine NO, Albro MB, Lima EG, Wei VI, Dubois CR, Hung CT, & Ateshian GA (2009). Effect of dynamic loading on the transport of solutes into agarose hydrogels. Biophysical Journal, 97(4), 968–975. doi:10.1016/j.bpj.2009.05.047 [PubMed: 19686643]

Charulatha V, & Rajaram A (2003). Influence of different crosslinking treatments on the physical properties of collagen membranes. Biomaterials, 24(5), 759–767. [PubMed: 12485794]

Chauhan VP, Stylianopoulos T, Martin JD, Popović Z, Chen O, Kamoun WS, … Jain RK (2012). Normalization of tumour blood vessels improves the delivery of nanomedicines in a size-dependent manner. Nature nanotechnology, 7, 383–388. doi:10.1038/nnano.2012.45

Chrobak KM, Potter DR, & Tien J (2006). Formation of perfused, functional microvascular tubes in vitro. Microvasc Res, 71(3), 185–196. doi:10.1016/j.mvr.2006.02.005 [PubMed: 16600313]

Chung M, Ahn J, Son K, Kim S, & Jeon NL (2017). Biomimetic Model of Tumor Microenvironment on Microfluidic Platform. Advanced Healthcare Materials, 6(15). doi:10.1002/adhm.201700196

Cummings CL, Gawlitta D, Nerem RM, & Stegemann JP (2004). Properties of engineered vascular constructs made from collagen, fibrin, and collagen-fibrin mixtures. Biomaterials, 25(17), 3699–3706. doi:10.1016/j.biomaterials.2003.10.073 [PubMed: 15020145]

Drury JL, & Mooney DJ (2003). Hydrogels for tissue engineering: scaffold design variables and applications. Biomaterials, 24(24), 4337–4351. [PubMed: 12922147]

Farahat WA, Wood LB, Zervantonakis IK, Schor A, Ong S, Neal D, … Asada HH (2012). Ensemble analysis of angiogenic growth in three-dimensional microfluidic cell cultures. PLoS One, 7(5), e37333. doi:10.1371/journal.pone.0037333 [PubMed: 22662145]

Fukumura D, & Jain RK (2007). Tumor microenvironment abnormalities: causes, consequences, and strategies to normalize. J Cell Biochem, 101(4), 937–949. doi:10.1002/jcb.21187 [PubMed: 17171643]

Gadde M, Marrinan D, Michna RJ, & Rylander MN (2018). Three Dimensional In Vitro Tumor Platforms for Cancer Discovery In Soker S & Skardal A (Eds.), Tumor Organoids (pp. 71–94): Springer International Publishing.

Galie PA, Nguyen D-HT, Choi CK, Cohen DM, Janmey PA, & Chen CS (2014). Fluid shear stress threshold regulates angiogenic sprouting. Proceedings of the National Academy of Sciences of the United States of America, 111, 7968–7973. doi:10.1073/pnas.1310842111 [PubMed: 24843171]

Galmarini FC, Galmarini CM, Sarchi MI, Abulafia J, & Galmarini D (2000). Heterogeneous distribution of tumor blood supply affects the response to chemotherapy in patients with head and neck cancer. Microcirculation, 7(6 Pt 1), 405–410. [PubMed: 11142337]

Ghousifam N, Mortazavian H, Bhowmick R, Vasquez Y, Blum FD, & Gappa-Fahlenkamp H (2017). A three-dimensional in vitro model to demonstrate the haptotactic effect of monocyte chemoattractant protein-1 on atherosclerosis-associated monocyte migration. Int J Biol Macromol, 97, 141–147. doi:10.1016/j.ijbiomac.2016.12.072 [PubMed: 28041913]

Gkretsi V, Zacharia LC, & Stylianopoulos T (2017). Targeting Inflammation to Improve Tumor Drug Delivery. Trends Cancer, 3(9), 621–630. doi:10.1016/j.trecan.2017.07.006 [PubMed: 28867166]

Golden AP, & Tien J (2007). Fabrication of microfluidic hydrogels using molded gelatin as a sacrificial element. Lab Chip, 7(6), 720–725. doi:10.1039/b618409j [PubMed: 17538713]

Griffith LG, & Swartz MA (2006). Capturing complex 3D tissue physiology in vitro. Nat Rev Mol Cell Biol, 7(3), 211–224. doi:10.1038/nrm1858 [PubMed: 16496023]

Grimes DR, Kannan P, McIntyre A, Kavanagh A, Siddiky A, Wigfield S, … Partridge M (2016). The Role of Oxygen in Avascular Tumor Growth. PLoS One, 11(4), e0153692. doi:10.1371/journal.pone.0153692 [PubMed: 27088720]

Hashizume H, Baluk P, Morikawa S, McLean JW, Thurston G, Roberge S, … McDonald DM (2000). Openings between defective endothelial cells explain tumor vessel leakiness. Am J Pathol, 156(4), 1363–1380. doi:10.1016/s0002-9440(10)65006-7 [PubMed: 10751361]

Ho YT, Adriani G, Beyer S, Nhan PT, Kamm RD, & Kah JCY (2017). A Facile Method to Probe the Vascular Permeability of Nanoparticles in Nanomedicine Applications. Sci Rep, 7(1), 707. doi:10.1038/s41598-017-00750-3 [PubMed: 28386096]

Hoffmann A, Bredno J, Wendland M, Derugin N, Ohara P, & Wintermark M (2011). High and Low Molecular Weight Fluorescein Isothiocyanate (FITC)-Dextrans to Assess Blood-Brain Barrier Disruption: Technical Considerations. Transl Stroke Res, 2(1), 106–111. doi:10.1007/s12975-010-0049-x [PubMed: 21423333]

Horning JL, Sahoo SK, Vijayaraghavalu S, Dimitrijevic S, Vasir JK, Jain TK, … Labhasetwar V (2008). 3-D tumor model for in vitro evaluation of anticancer drugs. Mol Pharm, 5(5), 849–862. doi:10.1021/mp800047v [PubMed: 18680382]

Huang YL, Segall JE, & Wu M (2017). Microfluidic modeling of the biophysical microenvironment in tumor cell invasion. Lab Chip, 17(19), 3221–3233. doi:10.1039/c7lc00623c [PubMed: 28805874]

Hutmacher DW, Horch RE, Loessner D, Rizzi S, Sieh S, Reichert JC, … Kneser U (2009). Translating tissue engineering technology platforms into cancer research. J Cell Mol Med, 13(8a), 1417–1427. doi:10.1111/j.1582-4934.2009.00853.x [PubMed: 19627398]

Jain RK (1988). Determinants of tumor blood flow: a review. Cancer Res, 48(10), 2641–2658. [PubMed: 3282647]

Jain RK, Martin JD, & Stylianopoulos T (2014). The role of mechanical forces in tumor growth and therapy. Annu Rev Biomed Eng, 16, 321–346. doi:10.1146/annurev-bioeng-071813-105259 [PubMed: 25014786]

Jang SH, Wientjes MG, Lu D, & Au JL (2003). Drug delivery and transport to solid tumors. Pharm Res, 20(9), 1337–1350. [PubMed: 14567626]

Jeon JS, Bersini S, Gilardi M, Dubini G, Charest JL, Moretti M, & Kamm RD (2015). Human 3D vascularized organotypic microfluidic assays to study breast cancer cell extravasation. Proc Natl Acad Sci U S A, 112(1), 214–219. doi:10.1073/pnas.1417115112 [PubMed: 25524628]

Jiang W, von Roemeling CA, Chen Y, Qie Y, Liu X, Chen J, & Kim BYS (2017). Designing nanomedicine for immuno-oncology. Nature Biomedical Engineering, 1, 0029. doi:10.1038/s41551-017-0029

Kamoun WS, Chae SS, Lacorre DA, Tyrrell JA, Mitre M, Gillissen MA, … Munn LL (2010). Simultaneous measurement of RBC velocity, flux, hematocrit and shear rate in vascular networks. Nat Methods, 7(8), 655–660. doi:10.1038/nmeth.1475 [PubMed: 20581828]

Kebers F, Lewalle JM, Desreux J, Munaut C, Devy L, Foidart JM, & Noel A (1998). Induction of endothelial cell apoptosis by solid tumor cells. Exp Cell Res, 240(2), 197–205. doi:10.1006/excr.1998.3935 [PubMed: 9596992]

Kolesky DB, Truby RL, Gladman AS, Busbee TA, Homan KA, & Lewis JA (2014). 3D bioprinting of vascularized, heterogeneous cell-laden tissue constructs. Adv Mater, 26(19), 3124–3130. doi:10.1002/adma.201305506 [PubMed: 24550124]

Landau LD, & Lifshitz EM (1987). Fluid Mechanics: Elsevier Science.

Lee H, Park W, Ryu H, & Jeon NL (2014). A microfluidic platform for quantitative analysis of cancer angiogenesis and intravasation. Biomicrofluidics, 8(5), 054102. doi:10.1063/1.4894595 [PubMed: 25332739]

Less JR, Skalak TC, Sevick EM, & Jain RK (1991). Microvascular architecture in a mammary carcinoma: branching patterns and vessel dimensions. Cancer Res, 51(1), 265–273. [PubMed: 1988088]

Ma L, Barker J, Zhou C, Li W, Zhang J, Lin B, … Honkakoski P (2012). Towards personalized medicine with a three-dimensional micro-scale perfusion-based two-chamber tissue model system. Biomaterials, 33(17), 4353–4361. doi:10.1016/j.biomaterials.2012.02.054 [PubMed: 22429982]

Ma Y-HV, Middleton K, You L, & Sun Y (2018). A review of microfluidic approaches for investigating cancer extravasation during metastasis. Microsystems &Amp; Nanoengineering, 4, 17104. doi:10.1038/micronano.2017.104

Mi S, Du Z, Xu Y, Wu Z, Qian X, Zhang M, & Sun W (2016). Microfluidic co-culture system for cancer migratory analysis and anti-metastatic drugs screening. Sci Rep, 6, 35544. doi:10.1038/srep35544 [PubMed: 27762336]

Mol A, van Lieshout MI, Dam-de Veen CG, Neuenschwander S, Hoerstrup SP, Baaijens FP, & Bouten CV (2005). Fibrin as a cell carrier in cardiovascular tissue engineering applications. Biomaterials, 26(16), 3113–3121. doi:10.1016/j.biomaterials.2004.08.007 [PubMed: 15603806]

Morgan JP, Delnero PF, Zheng Y, Verbridge SS, Chen J, Craven M, … Stroock AD (2013). Formation of microvascular networks in vitro. Nat Protoc, 8(9), 1820–1836. doi:10.1038/nprot.2013.110 [PubMed: 23989676]

Multhoff G, & Vaupel P (2012). Radiation-induced changes in microcirculation and interstitial fluid pressure affecting the delivery of macromolecules and nanotherapeutics to tumors. Front Oncol, 2, 165. doi:10.3389/fonc.2012.00165 [PubMed: 23162794]

Nagaraju S, Truong D, Mouneimne G, & Nikkhah M (2018). Microfluidic Tumor-Vascular Model to Study Breast Cancer Cell Invasion and Intravasation. Advanced Healthcare Materials. doi:10.1002/adhm.201701257

Nguyen DH, Stapleton SC, Yang MT, Cha SS, Choi CK, Galie PA, & Chen CS (2013). Biomimetic model to reconstitute angiogenic sprouting morphogenesis in vitro. Proc Natl Acad Sci U S A, 110(17), 6712–6717. doi:10.1073/pnas.1221526110 [PubMed: 23569284]

Niederhuber JE, Armitage JO, Doroshow JH, Kastan MB, & Tepper JE (2013). Abeloff's Clinical Oncology E-Book: Elsevier Health Sciences.

O'Brien FJ, Harley BA, Waller MA, Yannas IV, Gibson LJ, & Prendergast PJ (2007). The effect of pore size on permeability and cell attachment in collagen scaffolds for tissue engineering. Technology and Health Care: Official Journal of the European Society for Engineering and Medicine, 15, 3–17. [PubMed: 17264409]

Pagano G, Ventre M, Iannone M, Greco F, Maffettone PL, & Netti PA (2014). Optimizing design and fabrication of microfluidic devices for cell cultures: An effective approach to control cell microenvironment in three dimensions. Biomicrofluidics, 8. doi:10.1063/1.4893913

Parenteau-Bareil R, Gauvin R, & Berthod F (2010). Collagen-based biomaterials for tissue engineering applications. Materials, 3(3), 1863–1887.

Peela N, Truong D, Saini H, Chu H, Mashaghi S, Ham SL, … Nikkhah M (2017). Advanced biomaterials and microengineering technologies to recapitulate the stepwise process of cancer metastasis. Biomaterials, 133, 176–207. doi:10.1016/j.biomaterials.2017.04.017 [PubMed: 28437628]

Prabhakarpandian B, Shen M-C, Nichols JB, Garson CJ, Mills IR, Matar MM, … Pant K (2015). Synthetic Tumor Networks for Screening Drug Delivery Systems. Journal of controlled release : official journal of the Controlled Relea*se Society*, 201, 49–55. doi:10.1016/j.jconrel.2015.01.018 [PubMed: 25599856]

Pradhan S, Smith AM, Garson CJ, Hassani I, Seeto WJ, Pant K, … Lipke EA (2018). A Microvascularized Tumor-mimetic Platform for Assessing Anti-cancer Drug Efficacy. Sci Rep, 8. doi:10.1038/s41598-018-21075-9

Price GM, Chu KK, Truslow JG, Tang-Schomer MD, Golden AP, Mertz J, & Tien J (2008). Bonding of macromolecular hydrogels using perturbants. J Am Chem Soc, 130(21), 6664–6665. doi: 10.1021/ja711340d [PubMed: 18454530]

Price GM, & Tien J (2011). Methods for forming human microvascular tubes in vitro and measuring their macromolecular permeability. Methods Mol Biol, 671, 281–293. doi: 10.1007/978-1-59745-551-0_17 [PubMed: 20967637]

Price GM, Wong KH, Truslow JG, Leung AD, Acharya C, & Tien J (2010). Effect of mechanical factors on the function of engineered human blood microvessels in microfluidic collagen gels. Biomaterials, 31(24), 6182–6189. doi:10.1016/j.biomaterials.2010.04.041 [PubMed: 20537705]

Purtscher M, Rothbauer M, Holnthoner W, Redl H, & Ertl P (2015, 2015//). Establishment of Vascular Networks in Biochips Using Co-cultures of Adipose Derived Stem Cells and Endothelial Cells in a 3D Fibrin Matrix. Paper presented at the 6th European Conference of the International Federation for Medical and Biological Engineering, Cham.

Serpooshan V, Quinn TM, Muja N, & Nazhat SN (2013). Hydraulic permeability of multilayered collagen gel scaffolds under plastic compression-induced unidirectional fluid flow. Acta Biomater, 9(1), 4673–4680. doi:10.1016/j.actbio.2012.08.031 [PubMed: 22947324]

Shin Y, Han S, Jeon JS, Yamamoto K, Zervantonakis IK, Sudo R, … Chung S (2012). Microfluidic assay for simultaneous culture of multiple cell types on surfaces or within hydrogels. Nat Protoc, 7(7), 1247–1259. doi:10.1038/nprot.2012.051 [PubMed: 22678430]

Singleton PA (2014). Hyaluronan regulation of endothelial barrier function in cancer. Advances in Cancer Research, 123, 191–209. doi:10.1016/B978-0-12-800092-2.00007-1 [PubMed: 25081530]

Sleeboom JJF, Eslami Amirabadi H, Nair P, Sahlgren CM, & den Toonder JMJ (2018). Metastasis in context: modeling the tumor microenvironment with cancer-on-a-chip approaches. Disease Models & Mechanisms, 11. doi:10.1242/dmm.033100

Soleimani S, Shamsi M, Ghazani MA, Modarres HP, Valente KP, Saghafian M, … Sanati-Nezhad A (2018). Translational models of tumor angiogenesis: A nexus of in silico and in vitro models. Biotechnol Adv. doi:10.1016/j.biotechadv.2018.01.013

Song JW, Cavnar SP, Walker AC, Luker KE, Gupta M, Tung YC, … Takayama S (2009). Microfluidic endothelium for studying the intravascular adhesion of metastatic breast cancer cells. PLoS One, 4(6), e5756. doi:10.1371/journal.pone.0005756 [PubMed: 19484126]

Staton CA, Stribbling SM, Tazzyman S, Hughes R, Brown NJ, & Lewis CE (2004). Current methods for assaying angiogenesis in vitro and in vivo. Int J Exp Pathol, 85(5), 233–248. doi:10.1111/j.0959-9673.2004.00396.x [PubMed: 15379956]

Sung JH, Esch MB, Prot JM, Long CJ, Smith A, Hickman JJ, & Shuler ML (2013). Microfabricated mammalian organ systems and their integration into models of whole animals and humans. Lab Chip, 13(7), 1201–1212. doi:10.1039/c3lc41017j [PubMed: 23388858]

Sung KE, & Beebe DJ (2014). Microfluidic 3D models of cancer. Adv Drug Deliv Rev, 79-80, 68–78. doi:10.1016/j.addr.2014.07.002 [PubMed: 25017040]

Szot CS, Buchanan CF, Freeman JW, & Rylander MN (2011). 3D in vitro bioengineered tumors based on collagen I hydrogels. Biomaterials, 32(31), 7905–7912. doi:10.1016/j.biomaterials.2011.07.001 [PubMed: 21782234]

Szot CS, Buchanan CF, Freeman JW, & Rylander MN (2013). In vitro angiogenesis induced by tumor-endothelial cell co-culture in bilayered, collagen I hydrogel bioengineered tumors. Tissue Eng Part C Methods, 19(11), 864–874. doi:10.1089/ten.TEC.2012.0684 [PubMed: 23516987]

Tien J (2014). Microfluidic approaches for engineering vasculature. Current Opinion in Chemical Engineering, 3, 36–41.

Tong RT, Boucher Y, Kozin SV, Winkler F, Hicklin DJ, & Jain RK (2004). Vascular normalization by vascular endothelial growth factor receptor 2 blockade induces a pressure gradient across the vasculature and improves drug penetration in tumors. Cancer Res, 64(11), 3731–3736. doi: 10.1158/0008-5472.can-04-0074 [PubMed: 15172975]

Topper JN, & Gimbrone MA, Jr. (1999). Blood flow and vascular gene expression: fluid shear stress as a modulator of endothelial phenotype. Mol Med Today, 5(1), 40–46. [PubMed: 10088131]

Tourovskaia A, Fauver M, Kramer G, Simonson S, & Neumann T (2014). Tissue-engineered microenvironment systems for modeling human vasculature. Exp Biol Med (Maywood), 239(9), 1264–1271. doi:10.1177/1535370214539228 [PubMed: 25030480]

Tredan O, Galmarini CM, Patel K, & Tannock IF (2007). Drug resistance and the solid tumor microenvironment. J Natl Cancer Inst, 99(19), 1441–1454. doi:10.1093/jnci/djm135 [PubMed: 17895480]

Tsai H-F, Trubelja A, Shen AQ, & Bao G (2017). Tumour-on-a-chip: microfluidic models of tumour morphology, growth and microenvironment. Journal of The Royal Society Interface, 14, 20170137. doi:10.1098/rsif.2017.0137

Vaupel P, Kallinowski F, & Okunieff P (1989). Blood flow, oxygen and nutrient supply, and metabolic microenvironment of human tumors: a review. Cancer Res, 49(23), 6449–6465. [PubMed: 2684393]

Verbridge SS, Chandler EM, & Fischbach C (2010). Tissue-engineered three-dimensional tumor models to study tumor angiogenesis. Tissue Eng Part A, 16(7), 2147–2152. doi:10.1089/ten.TEA.2009.0668 [PubMed: 20214471]

Vickerman V, Blundo J, Chung S, & Kamm RD (2008). Design, Fabrication and Implementation of a Novel Multi Parameter Control Microfluidic Platform for Three-Dimensional Cell Culture and Real-Time Imaging. Lab on a Chip, 8, 1468–1477. doi:10.1039/b802395f [PubMed: 18818801]

Wang X, Li W, & Kumar V (2006). A method for solvent-free fabrication of porous polymer using solid-state foaming and ultrasound for tissue engineering applications. Biomaterials, 27, 1924–1929. doi:10.1016/j.biomaterials.2005.09.029 [PubMed: 16219346]

Whatcott CJ, Diep CH, Jiang P, Watanabe A, LoBello J, Sima C, … Han H (2015). Desmoplasia in Primary Tumors and Metastatic Lesions of Pancreatic Cancer. Clinical cancer research, 21, 3561–3568. doi:10.1158/1078-0432.CCR-14-1051 [PubMed: 25695692]

Whitesides GM, Ostuni E, Takayama S, Jiang X, & Ingber DE (2001). Soft lithography in biology and biochemistry. Annu Rev Biomed Eng, 3, 335–373. doi:10.1146/annurev.bioeng.3.1.335 [PubMed: 11447067]

Wong AD, & Searson PC (2014). Live-cell imaging of invasion and intravasation in an artificial microvessel platform. Cancer Res, 74(17), 4937–4945. doi:10.1158/0008-5472.can-14-1042 [PubMed: 24970480]

Wong KH, Truslow JG, Khankhel AH, Chan KL, & Tien J (2013). Artificial lymphatic drainage systems for vascularized microfluidic scaffolds. J Biomed Mater Res A, 101(8), 2181–2190. doi:10.1002/jbm.a.34524 [PubMed: 23281125]

Wong KH, Truslow JG, & Tien J (2010). The role of cyclic AMP in normalizing the function of engineered human blood microvessels in microfluidic collagen gels. Biomaterials, 31(17), 4706–4714. doi:10.1016/j.biomaterials.2010.02.041 [PubMed: 20303168]

Yamada KM, & Cukierman E (2007). Modeling tissue morphogenesis and cancer in 3D. Cell, 130(4), 601–610. [PubMed: 17719539]

Yamamura N, Sudo R, Ikeda M, & Tanishita K (2007). Effects of the mechanical properties of collagen gel on the in vitro formation of microvessel networks by endothelial cells. Tissue Eng, 13(7), 1443–1453. doi:10.1089/ten.2006.0333 [PubMed: 17518745]

Zervantonakis IK, Hughes-Alford SK, Charest JL, Condeelis JS, Gertler FB, & Kamm RD (2012a). Three-dimensional microfluidic model for tumor cell intravasation and endothelial barrier function. Proc Natl Acad Sci U S A, 109(34), 13515–13520. doi:10.1073/pnas.1210182109 [PubMed: 22869695]

Zervantonakis IK, Hughes-Alford SK, Charest JL, Condeelis JS, Gertler FB, & Kamm RD (2012b). Three-dimensional microfluidic model for tumor cell intravasation and endothelial barrier function. Proceedings of the National Academy of Sciences, 109(34), 13515–13520.

Zhang B, & Radisic M (2017). Organ-on-a-chip devices advance to market. Lab Chip, 17(14), 2395–2420. doi:10.1039/c6lc01554a [PubMed: 28617487]

Zheng Y, Chen J, Craven M, Choi NW, Totorica S, Diaz-Santana A, … Stroock AD (2012). In vitro microvessels for the study of angiogenesis and thrombosis. Proc Natl Acad Sci U S A, 109(24), 9342–9347. doi:10.1073/pnas.1201240109 [PubMed: 22645376]

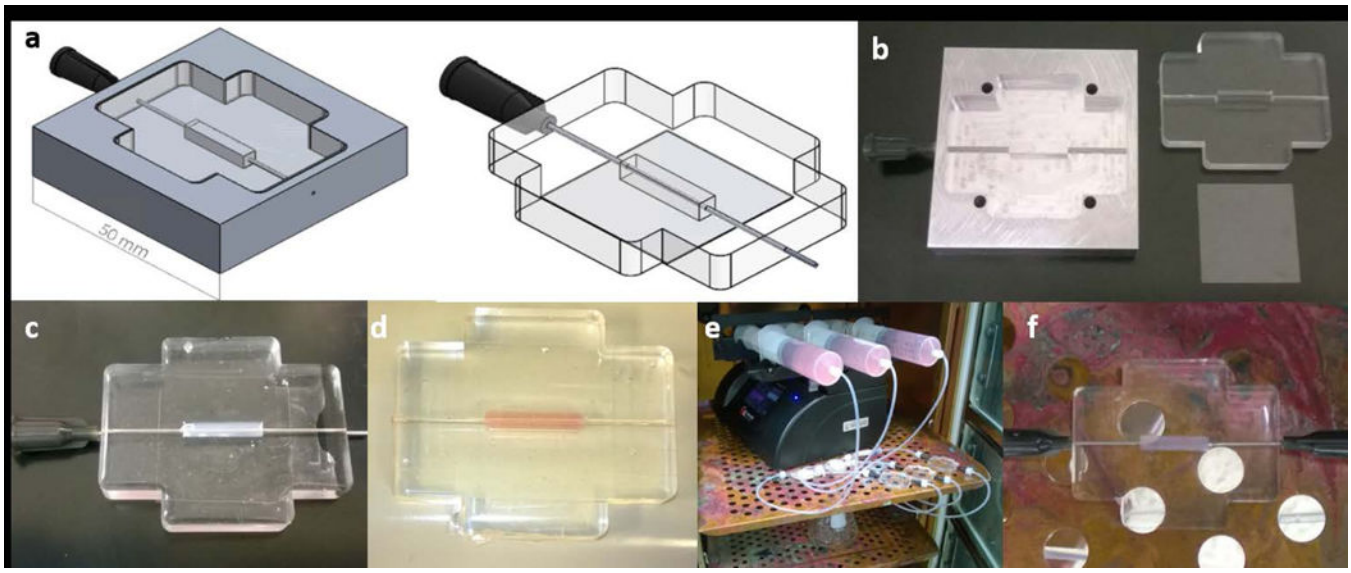

Figure 1:

Design of platform and fabrication of single vessel microfluidic collagen platform and perfusion setup. **(a)** CAD design of PDMS mold and PDMS tissue chamber with 22G inlets. **(b)** Machined aluminium mold, PDMS chamber produced from aluminium mold and glass. **(c)** Tissue chamber filled with collagen around a 22G needle. **(d)** Collagen hydrogel with channel after polymerization and removal of needle. **(e)** Setup of syringe pump flow system with bubble traps for perfusion through the hydrogel. **(f)** Close-up view of platform with 0.5” 22G needles inserted into the chamber inlet and outlet for preconditioning.

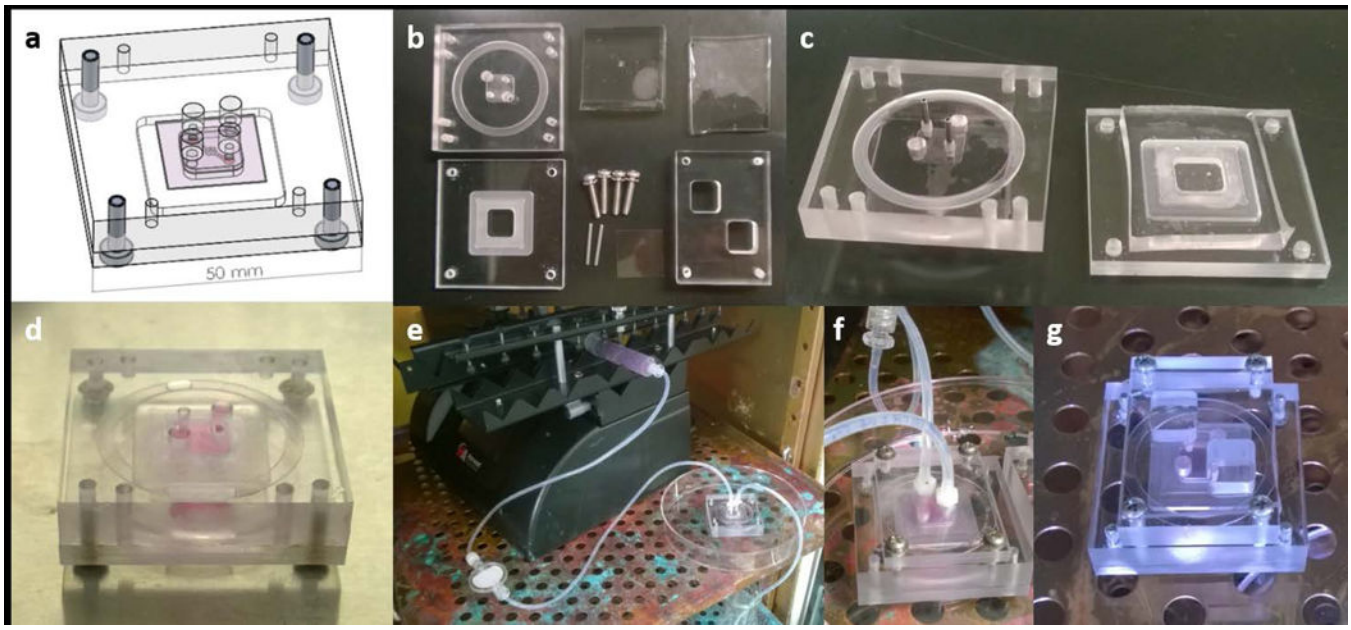

Figure 2:

Design of network platform and fabrication of microvascular network collagen hydrogels and perfusion setup. **(a)** CAD design of platform components and assembly. **(b)** Machined aluminium and polycarbonate components, PDMS stamps produced using lithographic techniques, and off the shelf parts. **(c)** Tissue chambers filled with collagen. **(d)** Collagen hydrogel with channel after polymerization and stacking of layers. **(e)** Setup of syringe pump flow system with bubble traps for perfusion through the network. **(f)** Close-up view of threaded inserts for attaching flow systems to the platform. **(g)** Gravity driven reservoir flow system.

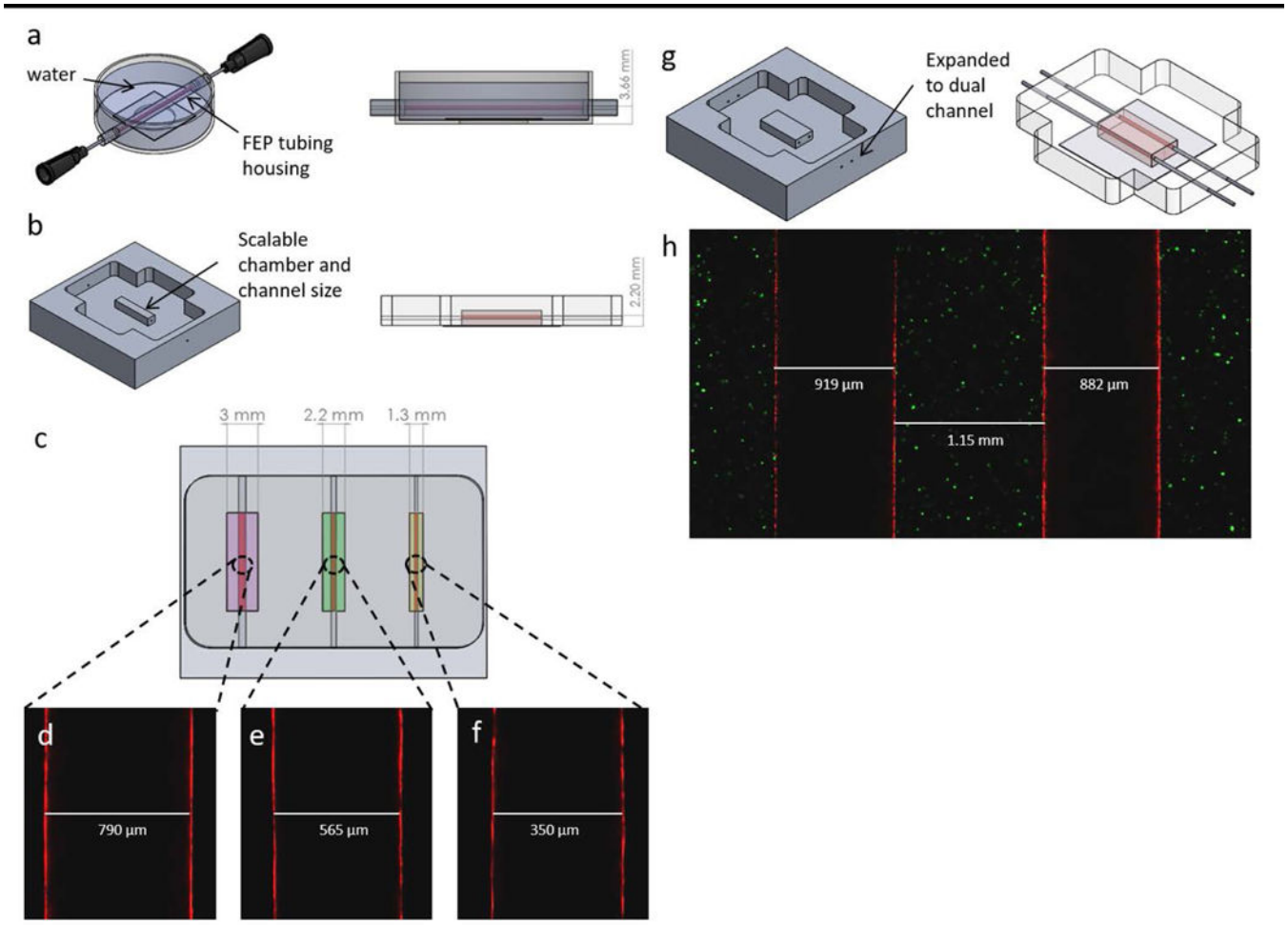

Figure 3:

Showcase of single vessel platform design improvements. **(a)** Original Rylander lab single vessel platform. **(b)** New scalable mold for making single vessel platforms. **(c)** CAD model of proposed multi-chamber vascularized tissue model. **(d-f)** Confocal single plane image of endothelialized vessels walls at the widest diameter formed using a 22, 25, and 30 gauge needle respectively. **(g)** Concept mold and platform for making dual channel platform. **(h)** Confocal single plane image of endothelialized 22 gauge dual channel tumor model.

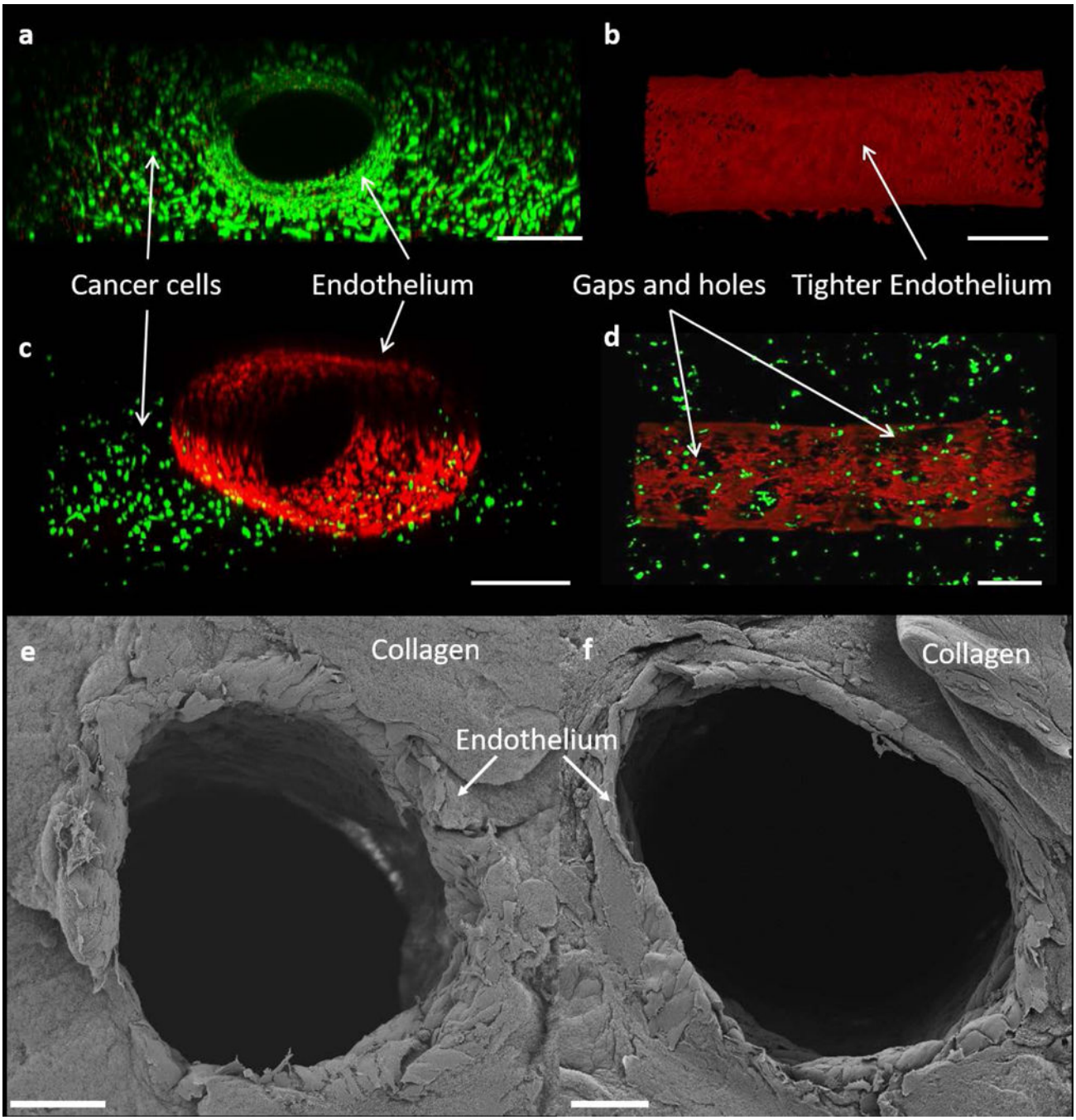

Figure 4:

Imaging of cell viability and confluence within the single vessel platform obtained upon immediate completion of preconditioning protocol and staining. **(a)** Front view of co-culture viability test, scale bar is 500 μm **(b)** Top view of f-actin stained mono-culture endothelium, scale bar is 500 μm. **(c)** Isometric 3D view of endothelium surrounded by cancer cells, scale bar is 500 μm. **(d)** Top view of f-actin stained endothelium in a co-culture environment, scale bar is 500 μm. **(e,f)** Cross sectional view of SEM images of the endothelium showing a

cylindrical endothelium in the TIME monoculture **(e)** and MDA-MB-231 and TIME cell co-culture **(f),** scale bars are 100 μm.

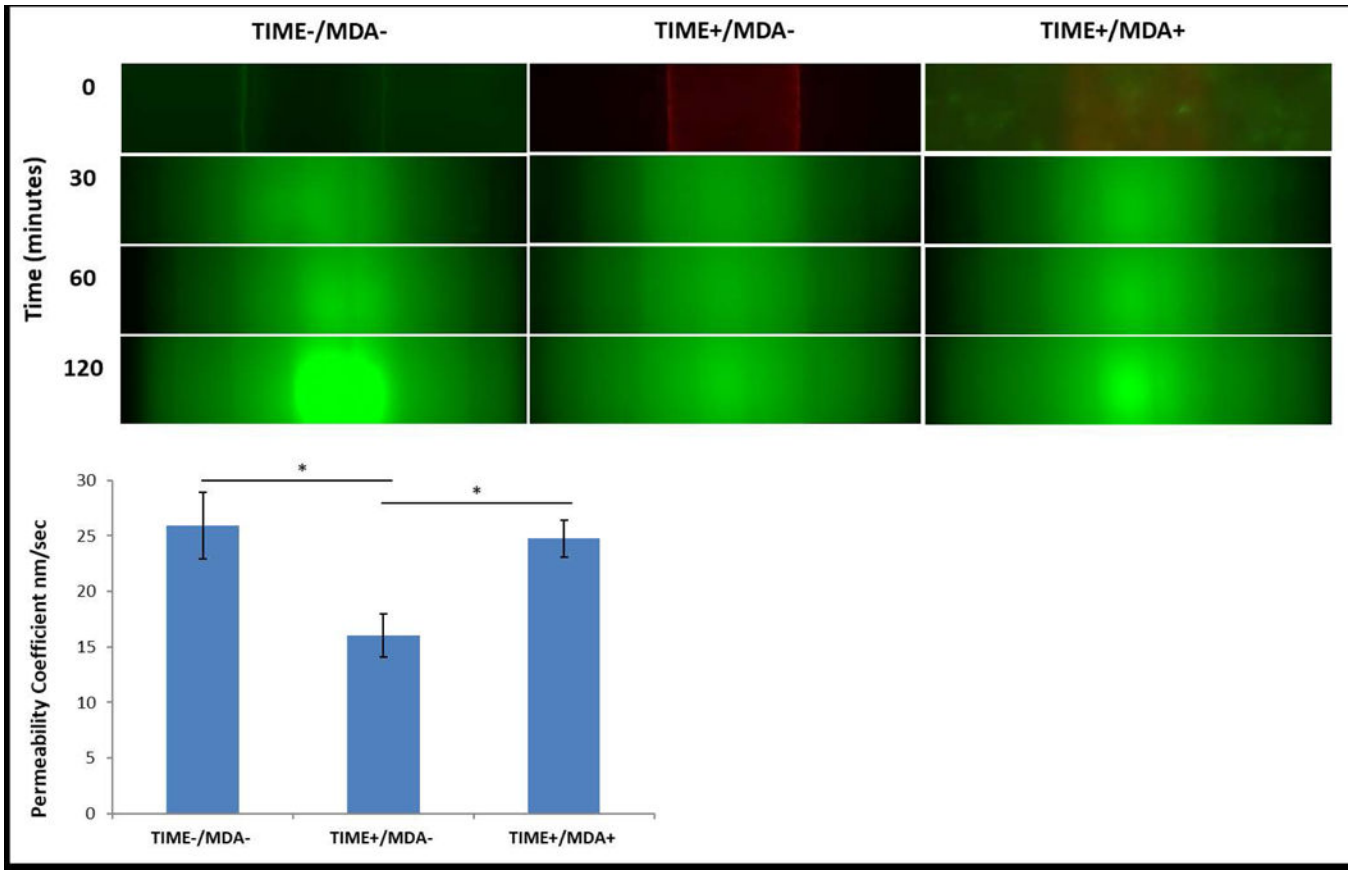

Figure 5:

Images of 70 kda green fluorescent dextran diffusing through a single vessel platform over 2 hours at a flow rate of 260 μl/min. Permeability coefficients after 2 hours of flow plotted for acellular, endothelium, and co-culture endothelium with cancer cells in the hydrogel (n=3, *p <0.05).

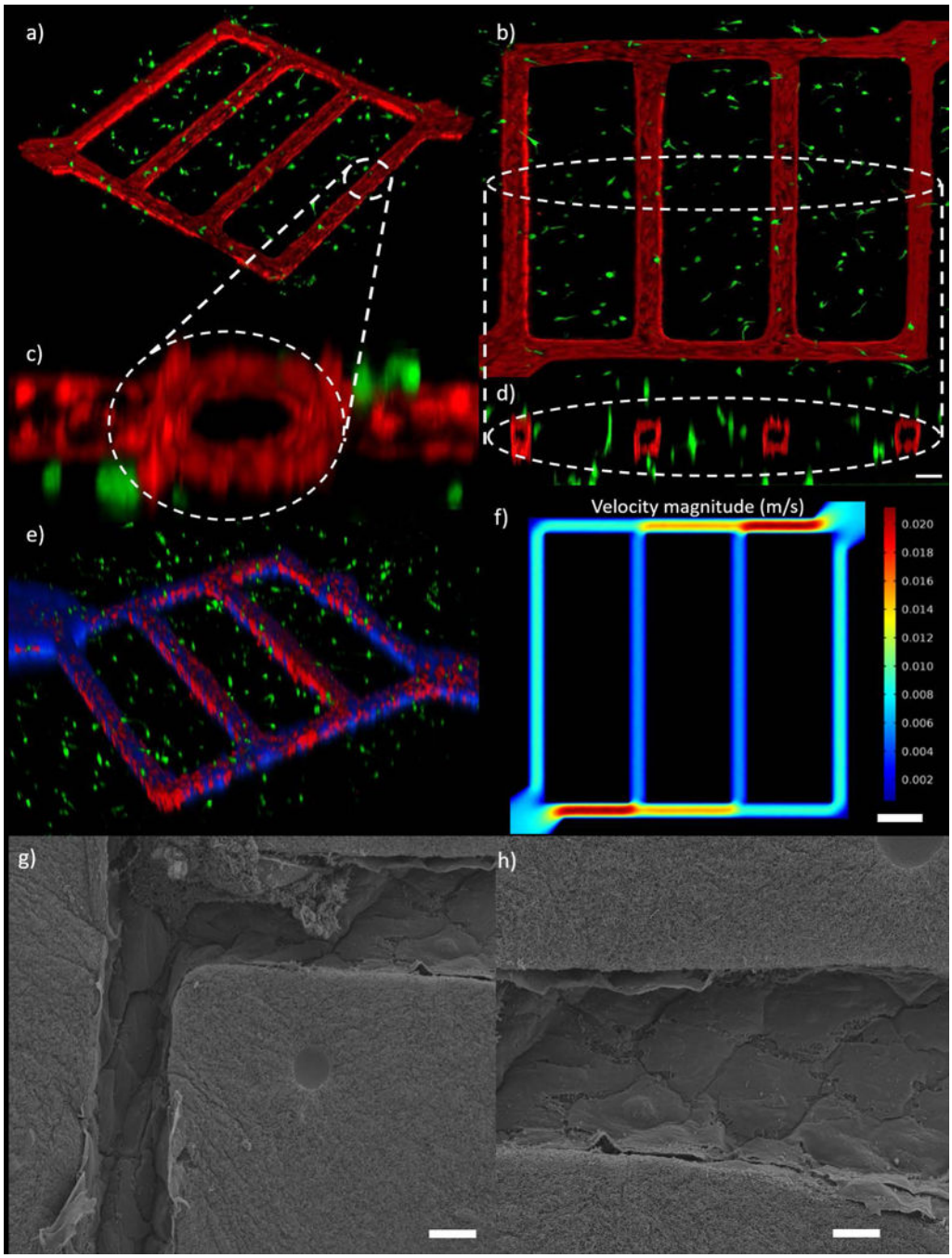

Figure 6:

In vitro tumor microenvironment microvascular network. **(a)** Isometric view of network co-culture of TIME cells and MDA-MB-231 cells. **(b)** Top view of the co-culture network **(c)** Cross section view of channel near inlet. **(d)** Cross section view of 4 channels, scale bar is 100 μm. **(e)** Transport of blue particles through the network. **(f)** Model predicted velocity magnitude inside tumor microenvironment microvascular network using finite element method, scale bar is 400 μm **(g, h)** SEM images the microchannels in the network platform

showing a patent and continuous endothelium at the corners **(g)** and in one of the channels **(h)**, scale bars are 20 μm.

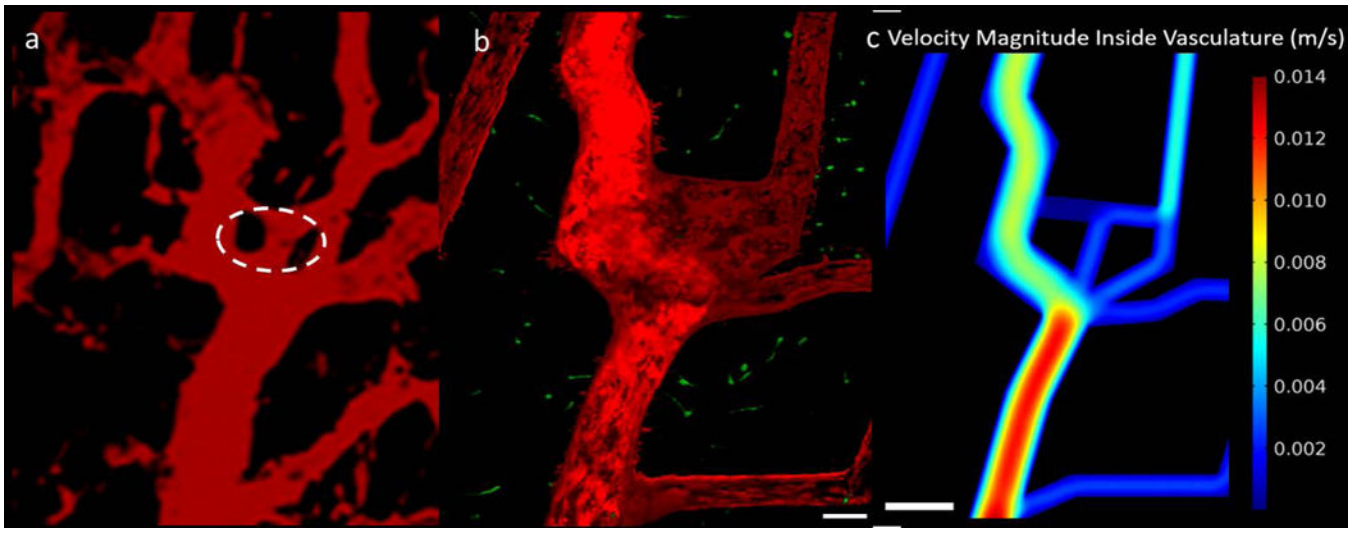

Figure 7:

In vitro recreation of an *in vivo* tumor. **(a)** two-photon image showing human colon carcinoma vasculature in mice at day 0 reproduced from Tong, R.T., Y. Boucher, S.V. Kozin, F. Winkler, D.J. Hicklin, and R.K. Jain. Vascular normalization by vascular endothelial growth factor receptor 2 blockade induces a pressure gradient across the vasculature and improves drug penetration in tumors. Cancer Res 64, 3731, 2004, with permission from AACR [60]. Circled region indicates areas difficult to recreate *in vitro*. **(b)** Engineered microfluidic tumor microenvironment capturing the geometry of an *in vivo* tumor, scale bar is 100 μm. **(c)** Obtained velocity magnitude inside in vivo tumor microenvironment microvascular using FEM simulations, scale bar is 500 μm.

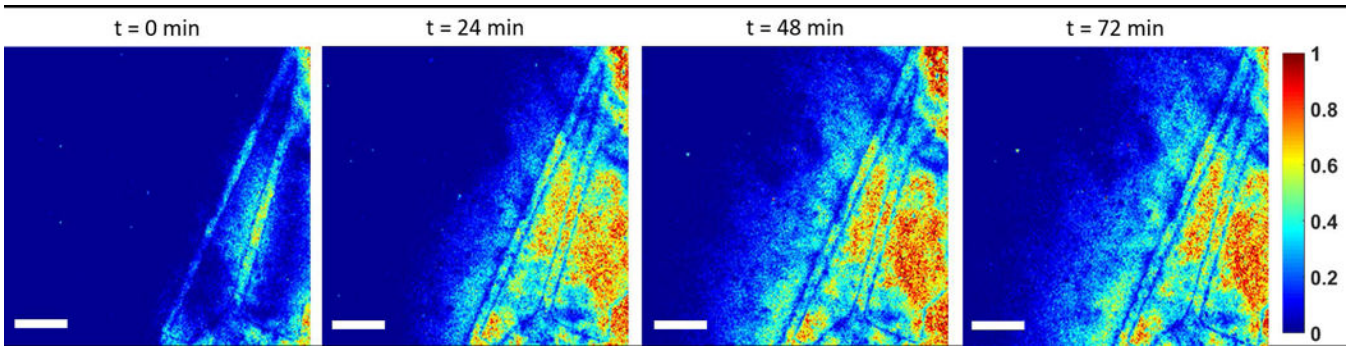

Figure 8:

Normalized intensity prolife of 70 kda dextran particles through *in vivo* vascular patterned platform as a function of time, scale bar is 400 μm.

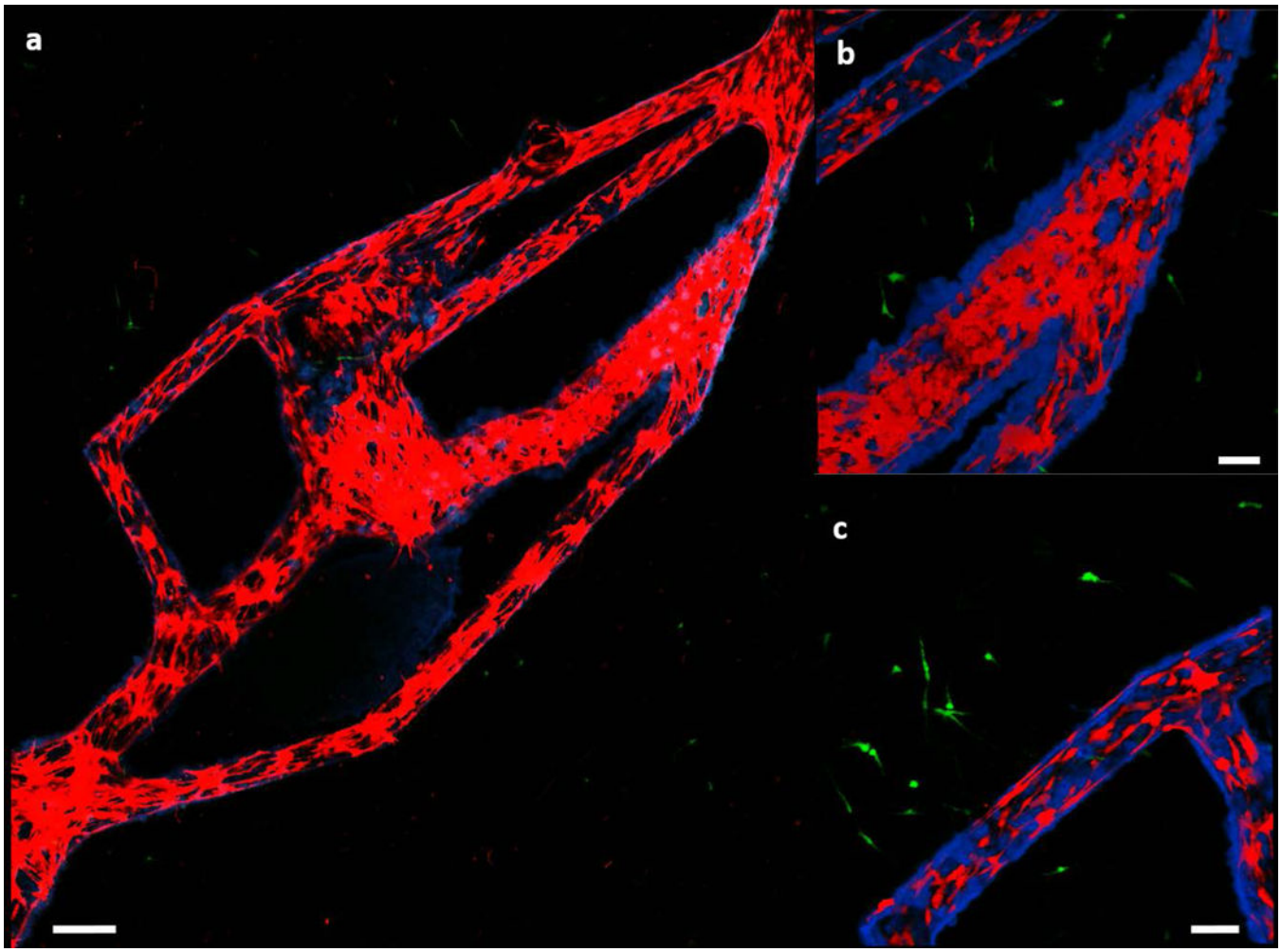

Figure 9:

(a) Transport of blue particles through the *in vivo* vascular patterned platform consisting of a co-culture of MDA-MB-231 cells (green) and TIME cells (red), scale bar is 250 μm. **(b,c)** Close up images of two different areas in the platform revealing aggregation of the particles, scale bars are 100 μm.